Comprehensive analysis of nasal IgA antibodies induced by intranasal administration of the SARS-CoV-2 spike protein.

Kentarou Waki [a] Hideki Tani [b], Yumiko Saga [b], Takahisa Shimada [b], Emiko Yamazaki [b], Seiichi Koike [c], Mana, Okada [d], Masaharu Isobe [c], Nobuyuki Kurosawa [c]

[a] Laboratory of Molecular and Cellular Biology, Graduate School of Science and Engineering for Education, University of Toyama, 3190 Gofuku, Toyama- shi, Toyama, 930-8555, Japan

[b] Department of Virology, Toyama Institute of Health, Toyama, Japan

[c] Laboratory of Molecular and Cellular Biology, Graduate School of Innovative Life Science, University of Toyama, 3190 Gofuku, Toyama- shi, Toyama, 930-8555, Japan

[d] Laboratory of Molecular and Cellular Biology, Faculty of Engineering, University of Toyama, 3190 Gofuku, Toyama- shi, Toyama, 930-8555, Japan

Corresponding author: Nobuyuki Kurosawa

E mail: kurosawa@eng.u-toyama.ac.jp

Laboratory of Molecular and Cellular Biology, Graduate School of Innovative Life Science, University of Toyama, 3190 Gofuku, Toyama- shi, Toyama, 930-8555, Japan

Abstract:

Intranasal vaccination is an attractive strategy for preventing COVID-19 disease as it stimulates the production of multimeric secretory immunoglobulin A (IgAs), the predominant antibody isotype in the mucosal immune system, at the target site of severe acute respiratory syndrome coronavirus 2 (SARS-CoV-2) entry. Currently, the evaluation of intranasal vaccine efficacy is based on the measurement of polyclonal antibody titers in nasal lavage fluid. However, how individual multimeric secretory IgA protects the mucosa from SARS-CoV-2 infection remains to be elucidated. To understand the precise contribution and molecular nature of multimeric secretory IgAs induced by intranasal vaccines, we developed 99 monoclonal IgAs from nasal mucosa and 114 monoclonal IgAs or IgGs from nonmucosal tissues of mice that were intranasally immunized with the SARS-CoV-2 spike protein. The nonmucosal IgAs exhibited shared origins and both common and unique somatic mutations with the related nasal IgA clones, indicating that the antigen-specific plasma cells in the nonmucosal tissues originated from B cells stimulated at the nasal mucosa. Comparing the spike protein binding reactivity, angiotensin-converting enzyme-2-blocking and SARS-CoV-2 virus neutralization of monomeric and multimeric IgA pairs recognizing different epitopes showed that even nonneutralizing monomeric IgA, which represents 70% of the nasal IgA repertoire, can protect against SARS-CoV-2 infection when expressed as multimeric secretory IgAs. Our investigation is the first to demonstrate the function of nasal IgAs at the monoclonal level, showing that nasal immunization can provide effective immunity against SARS-CoV-2 by inducing multimeric secretory IgAs at the target site of virus infection.

Introduction

Immunoglobulin A (IgA) is differentially distributed between the systemic and mucosal immune systems (*Li et al. , 2020*). Monomeric IgA (M-IgA) is predominantly present in serum, whereas secretory IgA (S-IgA) is the most prevalent IgA in mucous secretions. S-IgA is composed of two IgA units and one J chain, which are synthesized and assembled in local plasma cells. Secretory components expressed on the basolateral surface of mucosal epithelial cells bind the IgA complex through the J chain and transport the molecule to the apical cell membrane (*Woof and Kerr, 2006*). Recent studies have shown that S-IgA in the nasal mucosa exists not only as dimers but also as multimers (trimers and tetramers) in the human upper respiratory mucosa (*Saito et al. , 2019*). S-IgA plays an important role in the protection and homeostatic regulation of the airway, intestinal and vaginal epithelium through a process known as immune exclusion and immunosuppression (*Matsumoto, 2022*). Many studies have shown that S-IgA on mucosal surfaces is more effective and more cross-protective than IgG in serum for protection from harmful pathogens (*Okuya et al. , 2020b*) (*Asahi et al. , 2002*) (*Dhakal et al. , 2018*) (*Asahi-Ozaki et al. , 2004*).

COVID-19 is a disease caused by infection with severe acute respiratory syndrome coronavirus 2 (SARS-

CoV-2) that causes mild upper respiratory symptoms in most cases, but some patients develop bilateral pneumonia with acute respiratory distress (*Budinger et al. , 2021*). The SARS-COV-2 spike protein expressed on the virus surface is a multidomain homotrimer protein composed of an S1 domain consisting of an N-terminal domain (NTD) and receptor binding domain (RBD) and an S2 domain that mediates fusion of the virus and host cell membrane. Viral infection is initiated through the interaction between the RBD and the host receptor angiotensin-converting enzyme-2 (ACE2) (*Jackson et al. , 2022*). Thus, the spike protein is the main target for current vaccine development because antibodies against this protein can neutralize the infection. Currently approved intramuscular COVID-19 vaccines predominantly induce a systemic immune response by producing IgG in serum before they cause severe tissue damage, resulting in a high degree of efficacy (*Polack et al. , 2020*). However, these vaccines mainly induce IgG and M-IgA in serum; they do not induce S-IgA, which coats the upper respiratory tract mucosal surface (*DeFrancesco, 2020*). The emergence of highly infectious SARS-CoV-2 omicron variants may undermine the therapeutic efficacy of vaccines, requiring more effective vaccination to prevent SARS-CoV-2 infection. Since nasal epithelial cells are a primary target for SARS-CoV-2, intranasal vaccinations that induce S-IgA in the upper respiratory tract are desirable for protection against the infection and transmission of the virus (*Sungnak et al. , 2020*). To date, some intranasal vaccines are under development and have shown a robust mucosal and humoral immune responses in human and animal models (*Houston, 2023*) (*Chavda et al. , 2021*) (*Alu et al. , 2022*) (*Barrett et al. , 2021, Bricker et al. , 2021, D'Arco et al. , 2021, Kim et al. , 2021*) (*Vabret et al. , 2020*) (*Ohtsuka et al. , 2021*). Considerable efforts have been made to develop mucosal vaccines against pathogens, and nasal lavage fluids containing polyclonal S-IgAs have been used to evaluate the response to these vaccinations (*Maltseva et al. , 2022*) (*Gianchecchi et al. , 2019*) (*Wong et al. , 2022*) (*Afkhami et al. , 2022*) (*Sui et al. , 2021*) (*Azzi et al. , 2022*). However, it is difficult to obtain information regarding the functions of individual antibodies that comprise the polyclonal anti-viral mucosal repertoire from such broad assays. It has also been shown that intranasal vaccination induces a systemic antibody response, but the origin of these antibodies has not previously been investigated at the molecular level (*Tumpey et al. , 2001*).

To understand the precise contribution and molecular nature of S-IgA induced by intranasal vaccines with respect to its antiviral function, the development of monoclonal S-IgAs from plasma cells localized in nasal mucosa and studying their function is essential. However, because of the difficulties in developing monoclonal IgA antibodies from nasal mucosal tissue, many studies have used artificial switching of IgG to IgA for recombinant production, and this approach has been used to study the protective properties of IgA against pathogens (*Ejemel et al. , 2020, Saito et al. , 2019*). Such technological limitations have hampered the biochemical and clinical evaluation of intranasal vaccination at the molecular level. Our group has established robust protocols for the isolation of single antigen-specific plasma cells from a variety of animals and the high-throughput production of monoclonal antibodies (*Kurosawa et al. , 2012*).

Here, using this technology, we developed 213 antigen-specific monoclonal antibodies from plasma cells derived from mice that were intranasally immunized with a stabilized SARS-CoV-2 spike trimer protein (Spike) and demonstrated that intranasal immunization induced nasal-related antibodies in the spleen, lung, and blood. Analysis of the properties of monoclonal IgAs recognizing different epitopes revealed that multimerization of M-IgAs could induce neutralizing activity.

Results

Development of anti-Spike monoclonal M-IgAs from plasma cells localized in nasal mucosa.

To evaluate the immune response after the intranasal administration of the SARS-CoV-2 spike protein of the Wuhan-Hu-1/D614G strain ($Spike_{Wuhan}$), nasal lavage fluids and serum were collected from the mice one week after the last immunization. The intranasal administration of $Spike_{Wuhan}$ induced high levels of antigen-specific IgA but not IgG in nasal lavage fluids compared with those of the phosphate-buffered saline (PBS) control (Fig. 1A and Supplementary Fig.1).

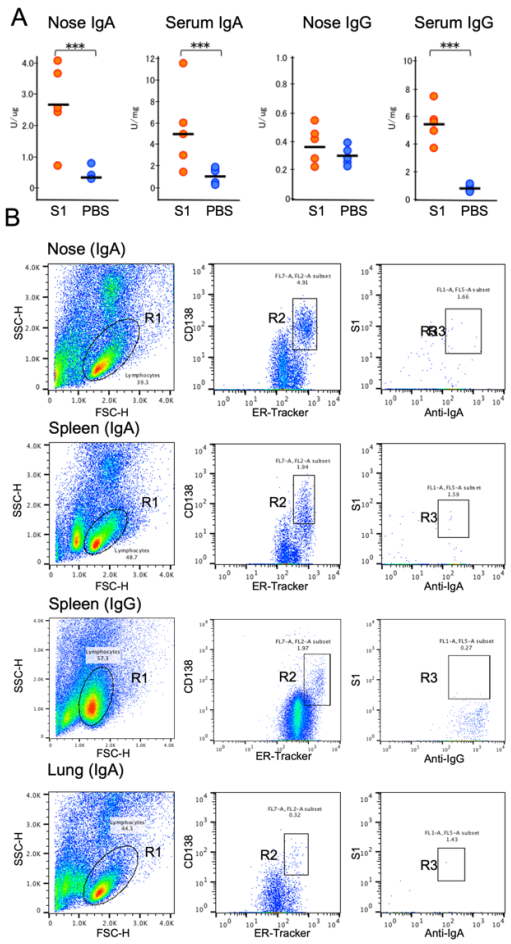

Fig. 1. Isolation of antigen-specific IgA$^+$ plasma cells from mice that were intranasally immunized with Spike$_{Wuhan}$.

(A) Mice were inoculated via the intranasal route with 10 μg of Spike$_{Wuhan}$ or PBS with 1 μg CT as an adjuvant. Nasal lavage fluid and serum were collected from the mice at one week after the last immunization, and antibody responses were evaluated using ELISA.

(B) FACS gating strategy for the isolation of S1-specific plasma cells from mice.

Cells from nasal mucosa or spleen were stained with anti-CD138, ER-tracker, anti-mouse IgA, and S1. Plots (I)-(III) represent the sequential gating strategy. (I) FSC vs. SSC with gate R1 representing lymphocytes. (II) The CD138$^+$ ER-Tracker^{High} fraction was defined as plasma cells. (R2). (III) The S1-specific plasma cells were defined as IgA$^+$, ER-Tracker^{High} and S1$^+$ (R3 gate). The numbers indicate the percentages of cells in the gated area. A total of 100,000 events were recorded. Representative data from the No. 1 mouse are shown.

Elevated levels of antigen-specific IgA and IgG responses were found in serum taken from the immunized mice, which is consistent with a previous study showing that intranasal vaccinations induce both nasal and serum IgA levels (*Sterlin et al. , 2021*) (*Maltseva et al. , 2022*). We selected three immunized mice with high nasal IgA titers and isolated antigen-specific plasma cells from the nasal mucosa, spleen, lung and blood. Cells isolated from these tissues were stained with fluorescently labeled anti-CD138, ER-tracker ER-Tracker Blue-White DPX, anti-IgA and S1 subunit of Spike$_{Wuhan}$ (S1), and then antigen-specific plasma cells defined as anti-CD138$^+$, ER-tracker^{high}, anti-IgA$^+$ and S1$^+$ were isolated by fluorescence-activated cell sorting (FACS). Consistent with the pattern of the IgA response observed in nasal lavage fluid, the proportions of antigen-specific IgA$^+$ plasma cells in the nasal mucosa of immunized mice were significantly higher than those of control mice (Fig. 1B and Supplementary file 1A).

Cognate pairs of immunoglobulin heavy chain variable (VH) and kappa light chain variable genes (VL) were amplified by rapid amplification of 5' cDNA ends PCR from the single-sorted cells. After constructing full-length immunoglobulin heavy and kappa light chain genes, antibodies were expressed by DNA transfection into CHO-S cells. Antigen-specific antibody clones were identified by enzyme-linked immunosorbent assay (ELISA) with immobilized Spike$_{Wuhan}$. After sequencing of the entire coding region of heavy and light chain genes, the antibodies sharing the same V-(D)-J genes were grouped (Supplementary Table 1). Then, representative antibody clones from each group were analyzed for their

binding to the spike protein RBD of Wuhan, Beta, Kappa and Delta variants and an NTD of Spike$_{Wuhan}$. The antibodies were also analyzed for their ability to block ACE2 binding to RBDs and to neutralize Wuhan pseudotyped virus. Based on their properties, each group of antibodies was arbitrarily categorized into five types. Type 1: anti-RBD, *ACE2 blocking* neutralizing *antibody; Type 2:* anti-RBD, *ACE2 blocking* nonneutralizing *antibody; Type 3:* anti-RBD, *non-ACE2 blocking* nonneutralizing *antibody; Type 4:* anti-NTD, *non-ACE-2 blocking* nonneutralizing *antibody; and Type 5: non-ACE-2 blocking* nonneutralizing *antibody targeting* epitopes other than RBD and NTD.

Intranasal immunization induces functionally diverse IgA in the nasal mucosa and spleen.

We conducted detailed characterization of antibodies obtained from the No. 1 mouse, as many antigen-specific M-IgA clones were obtained. Of the 51 nasal M-IgA clones analyzed, they were classified into 11 groups based on their V-(D)-J usage, with the majority (83%) clonally expanding into four major clusters (G2, G3, G4 and G10) and the remainder (17%) scattered across branches (Fig. 2A and B).

A

		RBD binding				NTD	ACE2-RBD blocking				Neutralize					
Type	Group	Wuhan	Beta	Kappa	Delta	Wuhan	Wuhan	Beta	Kappa	Delta	Wuhan	Nose	lung	spleen	Total	% of Clones
1	G1					−					+	1	0	0	1	0.9
1	G2					−					+	4	0	6	10	8.5
1	G3					−					+	12	0	5	17	14.5
1	G4					−					+	6	0	0	6	5.1
2	G5					−					−	1	0	2	3	2.6
2	G6					−					−	2	0	2	4	3.4
2	G7					−					−	1	0	0	1	0.9
2	G8					−					−	1	0	1	2	1.7
2	G9					−					−	2	0	0	2	1.7
3	G10					−					−	20	3	35	58	49.6
4	G11					+					−	1	0	0	1	0.9
UN		ND	ND	ND	ND	ND	ND	ND	ND	ND	ND	0	6	6	12	10.3
														Total	117	

>120 100-75 75-50 50-25 <25

B

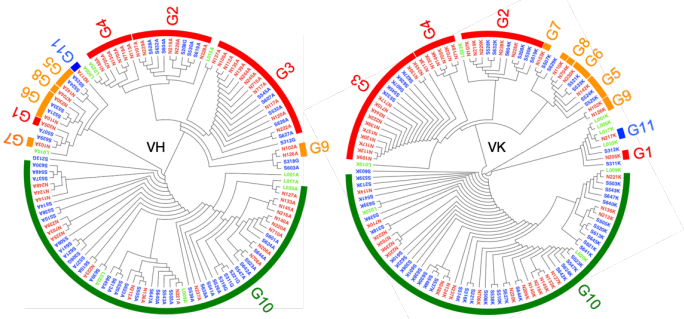

C

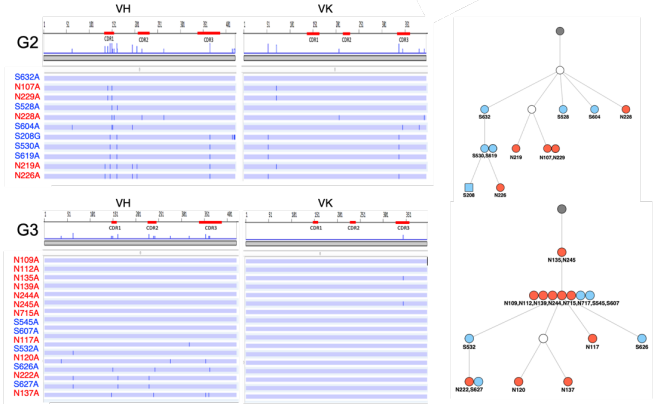

Fig. 2 Intranasal immunization induces functionally diverse antibodies in the nasal mucosa and spleen.

(A) Characterization of S1-specific monoclonal antibodies obtained from No. 1 mouse. The heatmap represents the relative intensity of antibody binding to RBDs and blocking of the RBD-ACE2 interaction. Blue (0–25%), green (25–50), orange (50–75%) and red (>75%). NTD binding was considered positive (+) when the OD at 405 nm was >0.3 after the background was subtracted. Neutralizing activity was considered positive (+) when the antibody suppressed Wuhan pseudotyped virus infection by 50%. The figure reports values from a single experiment. UN, antibody type not determined. ND, antibody activity not determined.

(B) Maximum-likelihood phylogenetic tree of the VH and VL chains of the S1-specific antibodies.

Different colored fonts indicate antibodies obtained from the nose (red), spleen (blue), and lung (green). Antibody groups are indicated by bands on the outer ring. The color of the band indicates antibody types: Type 1 (red), Type 2 (orange), Type 3 (green), Type 4 (blue) and Type 5 (gray). The antibody group is defined as clones using the same V-(D)-J usage and having an overall sequence identity of at least 95% from the signal peptide to framework 4 (FR4). The prefixes N, S and L in the antibody clone numbers refer to antibodies derived from the nose, spleen and lung, respectively. The suffixes A, G and K in the antibody clone numbers refer to alpha, gamma and kappa chain, respectively.

(C) Nucleotide sequence arraignment of VH and VL genes in the G2 and G3 antibodies form No. 1 mouse. The VH and VL sequences from the beginning of the signal peptide through the end of FR4 are shown as horizontal lines. Nucleotide changes relative to S632A and N109A are depicted as vertical bars across the horizontal lines. Different colored fonts indicate antibodies derived from the nose (red) and spleen (blue). Antibody phylogenetic trees based on VH/VK paired sequences are depicted. Gray circles represent the hypothetical germline configuration. White circles represent hypothetical ancestors. Colors indicate nasal (red) and splenic (blue) antibodies. Circles and squares indicate IgA and IgG, respectively.

The antibodies in the G1-G4 clusters were categorized as Type 1. The G1 antibody appeared only once. This clone displayed potent binding to the RBD of Wuhan, Kappa and Delta, and moderately to the Beta variant. It was also able to block ACE2 binding to all RBDs except the Beta variant RBD. The antibodies in G2-4 clusters bound to the RBD of Wuhan and Delta but not to the RBD of Beta and Delta. They were able to block ACE2 binding to the RBD of Wuhan and Delta but not to the RBD of Beta and Kappa. The antibodies in G5-G9 clusters were categorized as Type 2 and bound to all four RBD variants and

uniformly blocked ACE2 binding to the RBDs of all four strains. G10 antibodies were categorized as Type 3 and represented 38% of the nasal IgA repertoire. They bound to the RBDs of all four strains but failed to block ACE2 binding to the RBDs of all four strains. The G11 antibody was categorized as Type 4, was an anti-NTD antibody and did not block ACE2 binding to the RBDs of all four strains.

Intranasal immunization induces nasal-derived antibodies in the spleen, lung, and blood.

Previous reports suggest that nasopharynx-associated lymphoid tissue preferentially selects high-affinity IgA^+ B cells, which not only home back to regional mucosa but also migrate into nonmucosal tissues (*Shimoda et al. , 2001*). If this is the case, a fraction of S1-specific plasma cells differentiated from nasal-originated B cells may reside in the spleen and produce antibodies. To directly evaluate the cellular origin of the anti-S1 antibodies in nonmucosal tissues, we analyzed the presence of S1-specific plasma cells in the spleen, lung, bone marrow and Peyer's patches. FACS analysis of splenocytes harvested from No. 1 mice showed the presence of S1-specific IgA^+ plasma cells, but the splenocytes harvested from control mice did not exhibit S1-specific IgA^+ plasma cells (Fig. 1B and Supplementary file 1B). Single-cell-based immunoglobulin gene cloning resulted in the successful production of 49 S1-specific monoclonal IgAs. DNA sequence analysis of these clones revealed significant clonal overlap between the nose and spleen. (Fig. 2A and B). Clonal overlap was found in the G2-G3, G5, G6 and G10 clusters, in which G10 possessed the most expanded splenic clones, as in the case of nasal IgA (Fig. 2). Further investigation was carried out to determine whether IgG^+ plasma cells that express nasal-derived IgA could be detected in the spleen. Although the number of antigen-specific IgG^+ plasma cells was limited, eight IgG clones specific for S1 were isolated, among which five were potentially nasal-derived. When we attempted to isolate antigen-specific IgA^+ plasma cells from the lung, nine S1-specific IgA clones were obtained, among which three were potentially nasal-derived. The gut mucosa and bone marrow possessed a large population of IgA^+ plasma cells. However, we could not detect S1-specific IgA^+ plasma cells in Peyer's patches and bone marrow (Supplementary file 1B).

Next, we focused on the expanded antibody groups G2, G3 and G10 to analyze the patterns of somatic hypermutation (SHM). We found complex patterns of shared and unique SHMs in antibodies obtained from the nose, spleen and lung. In G2, the VHs of the three splenic clones (S530A, S208G, and S619A) had the same sequence, except for framework 4 of an IgG clone (S208G) and had three shared SHMs with the nasal clones (N219A and N226A). In addition, the VKs of the three splenic clones and N226A had the same sequence. In Group 3, seven nasal clones (N109A, N112A, N135A, N139A, N244A, N245A and N715A) and two splenic clones (S545 and S607) were 100% identical in nucleotide sequence, with N135A and N245 differing from the other clones by only one nucleotide in their VKs (Fig. 2C). Sequence analysis of the most expanded group, Group 10, also demonstrated clonal overlap in the nose, lung and spleen. For example, the VHs of a nasal clone (N221), spleen clones (S647, S503, S640 and S543) and a lung clone

(L009) were 100% identical, with S647 differing from the other clones by only one nucleotide in VK (Supplementary file 2). Antibody lineage analysis of these clones suggests that each family of related antibodies originates from a common ancestor gene that waws subjected to class switching and SHM. We also developed S1-specific Abs from No. 2 and No. 3 mice and analyzed their sequences (Fig. 3 and Supplementary file 3).

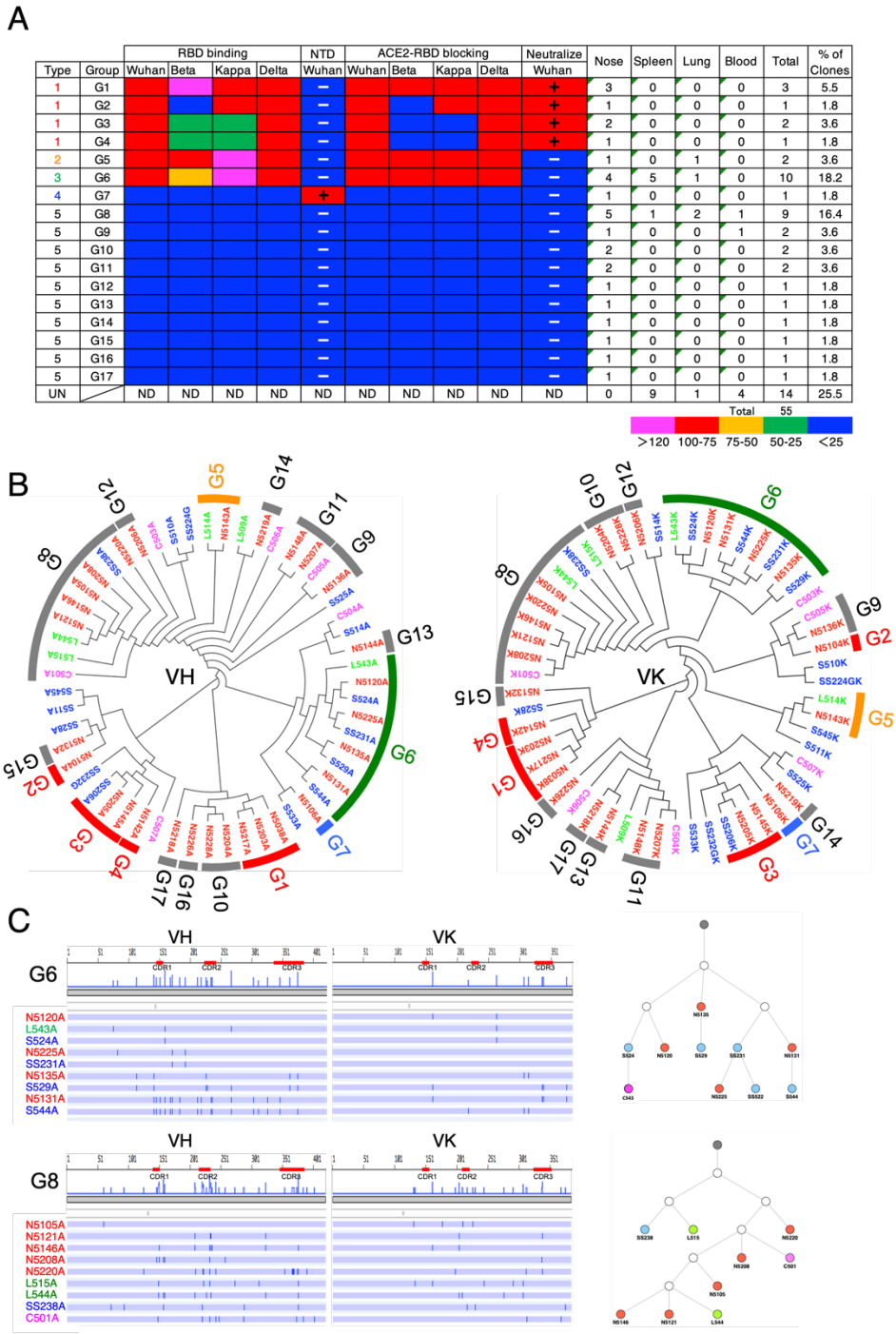

Type	Group	RBD binding Wuhan	RBD binding Beta	RBD binding Kappa	RBD binding Delta	NTD Wuhan	ACE2-RBD blocking Wuhan	ACE2-RBD blocking Beta	ACE2-RBD blocking Kappa	ACE2-RBD blocking Delta	Neutralize Wuhan	Nose	Spleen	Lung	Blood	Total	% of Clones
1	G1					−					+	3	0	0	0	3	5.5
1	G2					−					+	1	0	0	0	1	1.8
1	G3					−					+	2	0	0	0	2	3.6
1	G4					−					+	1	0	0	0	1	1.8
2	G5					−					−	1	0	1	0	2	3.6
3	G6					−					−	4	5	1	0	10	18.2
4	G7					+					−	1	0	0	0	1	1.8
5	G8					−					−	5	1	2	1	9	16.4
5	G9					−					−	1	0	0	1	2	3.6
5	G10					−					−	2	0	0	0	2	3.6
5	G11					−					−	2	0	0	0	2	3.6
5	G12					−					−	1	0	0	0	1	1.8
5	G13					−					−	1	0	0	0	1	1.8
5	G14					−					−	1	0	0	0	1	1.8
5	G15					−					−	1	0	0	0	1	1.8
5	G16					−					−	1	0	0	0	1	1.8
5	G17					−					−	1	0	0	0	1	1.8
UN		ND	ND	ND	ND	ND	ND	ND	ND	ND	ND	0	9	1	4	14	25.5

Total 55

>120 100-75 75-50 50-25 <25

Fig. 3. Characterization of S1-specific monoclonal antibodies obtained from No. 2 mouse.

(A) A total of 51 S1-reactive antibodies were analyzed for their properties as in Fig 2A. UN, antibody type not determined. ND, antibody activity not determined.

(B) Maximum-likelihood phylogenetic tree of the VH and VL chains of the S1-specific antibodies. Different colored fonts indicate antibodies obtained from the nose (red), spleen (blue), lung (green) and blood (magenta). Antibody groups are indicated by bands on the outer ring. The color of the band indicates antibody types: Type 1 (red), Type 2 (orange), Type 3 (green), Type 4 (blue) and Type 5 (gray). The prefixes N, S and L in the antibody clone numbers refer to antibodies derived from the nose, spleen and lung, respectively. The suffixes A, G and K in the antibody clone numbers refer to alpha, gamma and kappa chain, respectively.

(C) Nucleotide sequence arraignment of VH and VL genes in the G6 and G8 antibodies from No. 2 mouse. The. nucleotide changes relative to N5120A and N5105A are depicted as vertical bars across the horizontal lines. Different colored fonts indicate antibodies derived from nose (red), spleen (blue), lung (green) and blood (magenta). Antibody phylogenetic trees based on VH/VK paired sequences are depicted. Gray circles represent the hypothetical germline configuration. White circles represent hypothetical ancestors. Colors indicate nasal (red), splenic (blue), lung (green) and blood (magenta) antibodies.

In No. 2 mice, we obtained 29 nasal IgAs, 15 splenic antibodies (13 IgAs and two IgGs), five lung IgAs and six blood IgAs. They were classified into 17 groups based on their V-(D)-J usage, and each group was categorized as either Type 1, 2, 3, 4 or 5 based on antibody properties. (Fig. 3). Potentially nasal-derived clones were found in spleen, lung and blood (G5, 6, and 8). These clones also showed a complex pattern of shared and unique SHM with nasal clones throughout the full length of the VH and VL genes. In mouse No. 3, we cloned 19 nasal IgAs and 22 splenic antibodies (17 IgAs and five IgGs). They were classified into 10 groups, and each group was categorized as either Type 1, 3, 4 or 5. A high degree of clonal overlap between the nose and spleen was found, in which 13 out of 22 splenic Abs were potentially nasal-derived clones (Supplementary file. 3). Analysis of the VH and VL repertoires of the three mice revealed that the expanded clones constituted varying fractions of the antibody repertoire among different mice despite having received the same antigen, and no group of antibodies stood out across mice, suggesting that individual mice had immunologically distinct responses (Supplementary figure 4). In all mice, only a few bound to the NTD, and most of them were RBD-directed. Approximately 30% of M-IgAs categorized as Type 1 showed neutralizing activity (Supplementary figure 4). Taken together, regarding the mutation frequency and the pattern of SHM, it can be assumed that B cells stimulated by nasal challenges were the

major precursor of antigen-specific plasma cells in the spleen, lung and blood, which may contribute to antibody production in the lower respiratory tract and systemic circulation.

Multimerization of M-IgA enhances antigen-binding activity.

To examine how IgA multimerization affects antigen-binding activity, four representative clones (N5203, N142, N114 and N217) were selected from each type of antibody, and S-IgAs were expressed by cotransfecting alpha heavy chain, kappa light chain, J-chain and secretory component into CHO-S cells. Analysis of the purified S-IgAs by polyacrylamide gel electrophoresis (SDS–PAGE) revealed a band corresponding to the alpha heavy chain, kappa light chain and secretory component. Native PAGE analysis revealed bands corresponding to the dimer (~400 kDa), trimer (~550 kDa) and tetramer (~750 kDa) at a molar ratio of 5:1:3 (Fig. 4A).

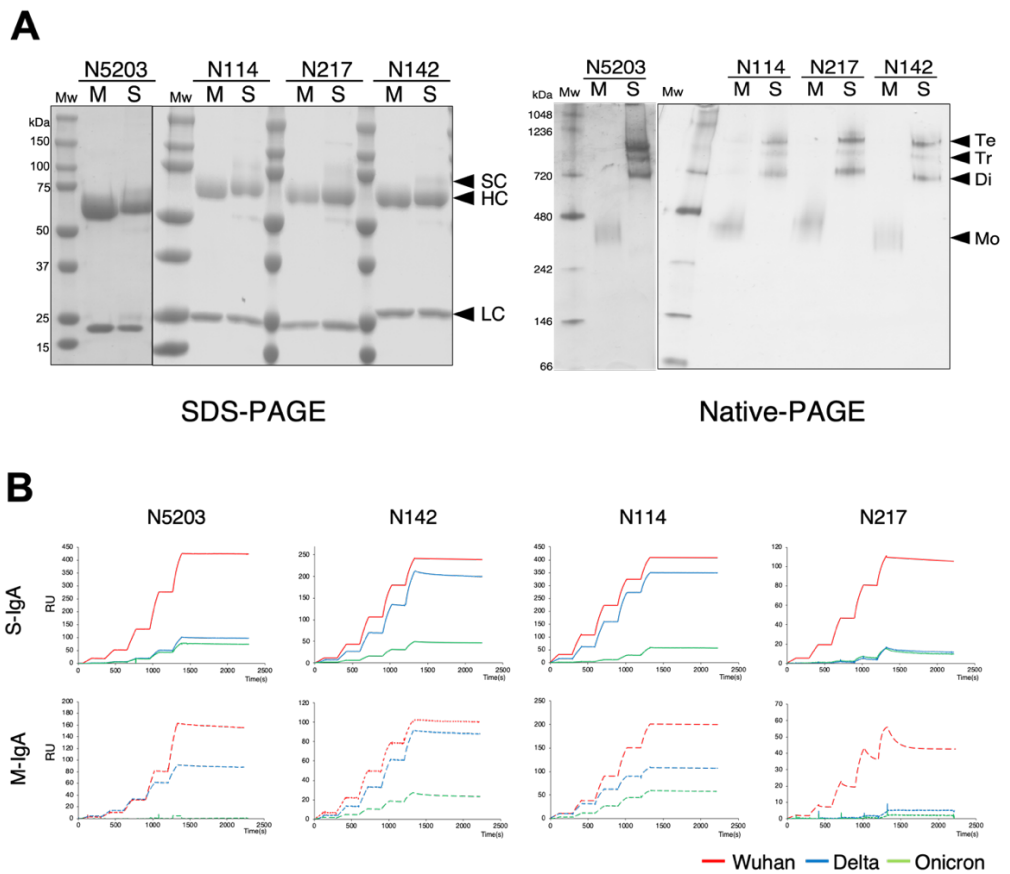

Strain	IgA	N5203			N142			N114			N217		
		Ka	Kd	KD	Ka	Kd	KD	Ka	Kd	KD	Ka	Kd	KD
Wuhan	S-IgA	9.0E+04	1.3E-07	1.3E-13	1.2E+06	4.0E-05	4.5E-11	1.9E+06	2.9E-06	2.0E-12	1.4E+06	8.7E-05	6.4E-11
	M-IgA	9.0E+03	4.6E-04	5.2E-09	6.3E+05	5.9E-05	9.5E-11	1.9E+06	4.0E-05	6.8E-11	3.4E+05	7.1E-03	2.1E-08
Delta	S-IgA	3.0E+05	6.4E-04	2.1E-09	8.9E+05	7.0E-05	7.8E-11	8.1E+05	6.3E-05	1.6E-10	ND	ND	ND
	M-IgA	3.0E+05	4.1E-04	2.4E-09	7.6E+05	6.5E-05	8.7E-11	5.2E+05	4.9E-05	9.7E-11	ND	ND	ND

Fig. 4 Comparison of reactivity between monomeric and multimeric IgAs.

(A) Production of recombinant M-IgAs and S-IgAs. Recombinant M-IgA and S-IgA purified from the culture supernatant of CHO cells were subjected to SDS–PAGE and Blue native-PAGE analysis. Bands corresponding to a monomer (M), dimer (Di), trimer (Ti) and tetramer (Te) are shown. H, α heavy chain; L, light chain; J, J chain; SC, secretory component; M, M-IgA; S, S-IgA

(B) Binding dynamics of M-IgAs and S-IgAs to Wuhan, Delta or Omicron spike protein by SPR. The curves shown are representative of two or three determinations. RU, resonance units. The table shows the association (ka) ($M^{-1}s^{-1}$), dissociation (kd) (s^{-1}) rate constants and apparent equilibrium dissociation constants (KD) expressed as the mean of two or three determinations (lower panel).

Then, we compared the binding kinetics of each pair of M-IgA/S-IgA by surface plasmon resonance (SPR) with immobilized $Spike_{Wuhan}$, $Spike_{Delta}$ or $Spike_{Omicron}$. As shown in Fig. 4B, N5203 M-IgA, which has moderate binding affinity to $Spike_{Wuhan}$ (apparent equilibrium constant, K_D=5.2E-9), acquired dramatic enhancement of the binding activity to $Spike_{Wuhan}$ after multimerization (K_D=1.3E-13). However, multimerization did not enhance the binding activity to $Spike_{Delta}$ (K_D=2.1E-9). N142 M-IgA, which has high affinity for $Spike_{Wuhan}$ (K_D=4.5E-11) and $Spike_{Delta}$ (K_D=7.8E-11), did not show enhanced binding activity to them after multimerization. Almost the same phenomenon was found for N114 M-IgA, which has high affinity for $Spike_{Wuhan}$ (K_D=6.8E-11) and $Spike_{Delta}$ (K_D=9.7E-11). N142 M-IgA, which has the lowest affinity to $Spike_{Wuhan}$ (K_D=2.1E-8), also acquired dramatic enhancement of the binding activity to $Spike_{Wuhan}$ after multimerization (K_D=6.4E-11) but not to $Spike_{Delta}$. All antibodies showed little or marginal levels of binding to $Spike_{Omicron}$. These results suggest that the degree of avidity of S-IgAs depends on the affinity of the parent monomeric antibody: antibodies with low or intermediate affinity in the monomeric state (N5203 and N217) can increase their avidity by multimerization but not antibodies with high affinity in the monomeric state (N142 and N114). These results are consistent with recent work by Saito, S. et al., who examined the function of multimerized IgA against influenza viruses (*Saito et al. , 2019*).

Multimerization facilitates stronger neutralization activity in nonneutralizing M-IgA

We next examined whether multimerization of IgAs influences the RBD-ACE2 interaction by competitive ELISA (Fig. 5A).

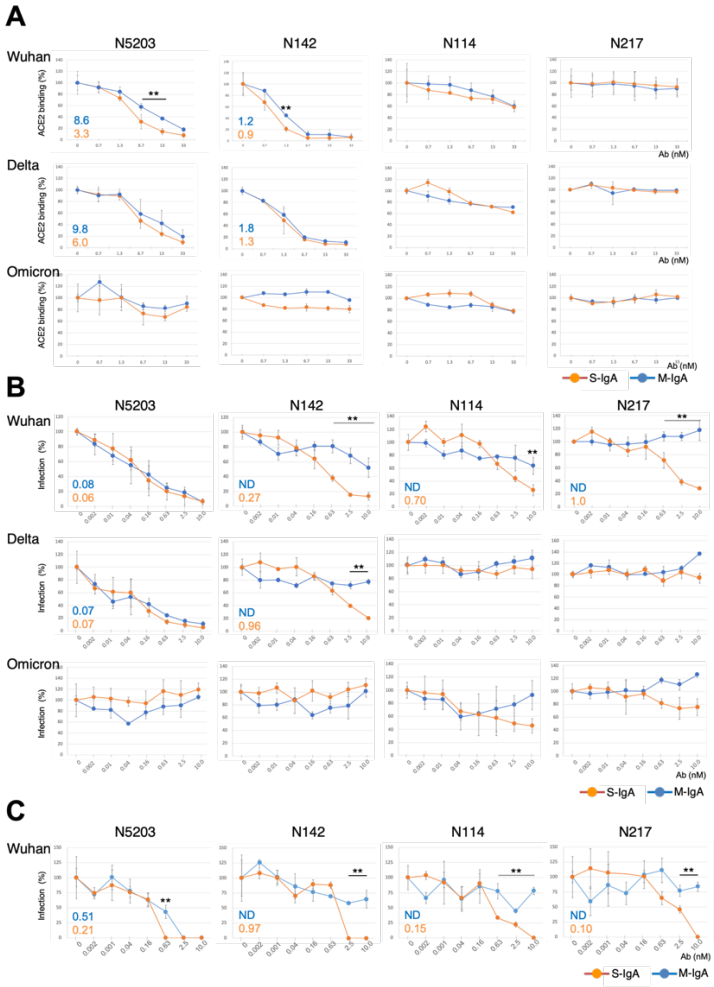

Fig. 5 Multimerization facilitates the neutralization activity of nonneutralizing M-IgAs.

(A) Graphs of the competitive ELISA results showing the binding of biotinylated ACE2 to the immobilized Wuhan, Delta or Omicron RBD in the presence of antibodies. The results are expressed as the mean ± SD of three technical replicates. The IC_{50} values of the indicated antibodies that inhibit the RBD-ACE2 interaction are shown in the diagrams.

(B) Comparison of neutralization activity between M-IgaA and S-IgA against SARS-CoV-2 pseudotyped viruses. Neutralization curves of the indicated antibody against pseudotyped viruses bearing spike proteins of Wuhan, Delta or Omicron are shown. Pseudotyped viruses preincubated with antibodies at the indicated concentrations were used to infect VeroE6 cells, and luciferase activities in cell lysates were measured at 20 h post transduction to calculate infection (%) relative to nonantibody-treated controls. The results are expressed as the mean ± SD of three technical replicates. The NT_{50} values of the indicated antibodies are shown in the diagrams. Antibodies that did not reach >70% inhibition at the highest concentration tested were listed as data not determined (ND).

(C) Comparison of neutralization potential between M-IgA and S-IgA against authentic SARS-CoV-2 BA.1. The neutralizing potential of the antibody was determined using an RT-PCR-based SARS-CoV-2 neutralization assay. VeroE6 cells preincubated with authentic SARS-CoV-2 BA.1 virus were incubated with the indicated antibodies at various concentrations. The virus in the cell culture medium was measured at 48 h post transduction to calculate infection (%) relative to nonantibody-treated controls. The results are expressed as the mean ± SD of three technical replicates. The NT_{50} values of the indicated antibodies are shown in the diagrams. Antibodies that did not reach >50% inhibition at the highest concentration tested are listed as ND. **$p<0.01$

Although the multimerization of N5203 M-IgA led to the dramatic enhancement of $Spike_{Wuhan}$ binding, it only increased RBD_{Wuhan}-ACE2 blocking by 3.3-fold, and there were no differences in RBD_{Delta}-ACE2 blocking between M-IgA and S-IgA. In N142 M-IgA, multimerization slightly increased RBD_{Wuhan}-ACE2 blocking but not RBD_{Delta}-ACE2 blocking. Multimerization of N114 and N217 M-IgA did not enhance RBD_{Wuhan}-ACE2 and RBD_{Delta}-ACE2 blocking, as in the case of their monomeric forms. None of the antibodies showed $RBD_{Omicron}$-ACE2 blocking even at the highest antibody concentrations. To analyze whether multimerization affects the functionality of M-IgAs, we tested all M-IgA/S-IgA pairs for their ability to neutralize pseudotyped lentiviruses bearing the Wuhan, Delta or Omicron spike protein. Both monomeric and multimeric forms of N5203 showed strong neutralizing activity against the Wuhan and Delta pseudotyped lentiviruses, but the concentrations required to achieve the 50% neutralizing titer (NT_{50}) were almost the same for both. Although both forms of N142 displayed RBD_{Wuhan}-ACE2 and RBD_{Delta}-ACE2 blocking, only the multimeric form showed neutralization activity against the Wuhan and Delta pseudotyped lentiviruses. Notably, N114 M-IgA and N217 M-IgA, which did not have RBD_{Wuhan}-ACE2 blocking activity, displayed neutralizing activity against the Wuhan but not the Delta pseudotyped lentivirus after multimerization. None of the antibodies exhibited neutralization activity against the Omicron pseudotyped lentivirus. We further tested the neutralization activity of these antibodies by using an authentic SARS-CoV-2 Wuhan strain. N5203 S-IgA showed twofold higher neutralization activity than its monomeric counterpart. As predicted from the results of the pseudotyped lentivirus assay, multimerization of N142, N114 and N217 M-IgA induced neutralization activity, while their monomeric counterparts failed to neutralize live virus at the highest antibody concentration. These results suggest that the neutralizing activity of S-IgAs is not solely attributed to the spike protein affinity and the RBD-ACE2 blocking activity of M-IgAs, and that the valence and binding mode between the epitope and paratope affect their function.

DISCUSSION

In this paper, we developed 99 antigen-specific monoclonal IgAs from the nasal mucosa of mice intranasally immunized with $Spike_{Wuhan}$ and demonstrated that immunization induces functionally diverse antibodies in nasal mucosa. We also cloned 114 antigen-specific antibodies from plasma cells localized in the spleen, lung and blood of the immunized mice, which revealed the presence of many potentially nasal-derived sequences. Analysis of the reactivity and functionality of the antibodies recognizing different epitopes revealed that multimerization facilitates the neutralizing activity of nonneutralizing M-IgAs. The different effects of multimerization suggest that each S-IgA has a different mechanism of action with respect to the suppression of SARS-CoV-2 infection, and the affinity, valence, and binding mode of the epitope and paratope may contribute to this variation.

It has been shown that the mucosal route of immunization elicits immune responses at local sites, as well as systemic immune responses. (*Lapuente et al. , 2021*). Our analysis demonstrated that the spleen possessed a larger population of antigen-specific plasma cells that expressed potentially nasal-derived IgAs and IgGs. These results suggest that the B cells activated in the nasal immune system give rise to plasma cells that reside in the nasal mucosa and produce S-IgA, while the B cells also migrate to the spleen and produce M-IgA. The role of the spleen in the induction of potentially nasal-derived antibodies by intranasal immunization is yet to be determined. The antigen specific plama cells in spleen may respond in cases of systemic infection by supplying M-IgAs and IgGs into the bloodstream or protecting the body against subsequent infection (*Afkhami et al. , 2022*) (*Sheikh-Mohamed et al. , 2022*). Although bone marrow and the intestines are reservoirs for IgA-producing B cells, we could not detect antigen-specific plasma cells in these tissues. The molecular mechanisms regulating potentially nasal-derived B-cell migration into the spleen but not into bone marrow and Peyer's patches remain to be determined.

To date, SARS-CoV-2 research has mainly focused on *anti-RBD* neutralizing antibodies, and the role of nonneutralizing antibodies has not been adequately analyzed. In this study, we demonstrated that nonneutralizing M-IgAs, which comprise 70% of the nasal IgA repertoire, showed strong neutralizing activity when expressed as S-IgAs. Our findings suggest that *factors other than the ability to block the ACE2 binding site of RBDs are involved in the neutralization activity of S-IgAs* (*Nicasio et al. , 2012*) (*Tan et al. , 2016*). Recent reports show that antibodies that induce inter- or intraspike crosslinking can inhibit viral binding or shedding by the host cell through steric hindrance or cause conformational changes in the spike proteins (*Galimidi et al. , 2015*) (*Jackson et al. , 2022*) (*Klein and Bjorkman, 2010*). Such inter- and intraspike cross-linking may be limited in M-IgAs if the spike protein density on the virus surface is low or if the epitopes are unfavorably located. We hypothesize that S-IgA could exert the above effects through its multivalent arms, a mode of action that is hard to achieve with M-IgA, and factors such as valency, epitope selection, antibody binding angle, and the bulkiness of the Fc are involved in this process. (*Okuya et al. , 2020a*) (*Callegari et al. , 2022*).

There are limitations of our study, including the number of antigen-specific plasma cells isolated from the nasal mucosa of immunized mice was insufficient for a comprehensive analysis of systemic and mucosal immune responses. In this study, antibodies that did not share V-(D)-J with nasal clones were found in the spleen, lungs and blood of immunized mice. This finding was probably due to the limited number of clones that was isolated from the nose. However, we cannot exclude the possibility that these clones were differentiated from local naïve B cells.

In conclusion, our study highlights the key role of S-IgA in the protective effect of mucosal immunity, which may be useful for better understanding how intranasal vaccines can help protect against SARS-CoV-2 infection.

Materials and methods

Study approval

All experiments were performed in accordance with relevant guidelines and regulations. Animal experimental protocols were approved by the Committee on Animal Experimentation at the University of Toyama and conducted using project license A2017eng-1.

Materials

The materials used in this study can be found in the Supplementary Ma. VeroE6/TMPRSS2 cells were purchased from the Japanese Collection of Research Bioresources (JCRB) Cell Bank (the National Institute of Biomedical Innovation, Health, and Nutrition, Osaka, Japan) (JCRB1819). Female ICR mice were purchased from Japan SLC, Inc. (Tokyo, Japan).

Immunization

Anesthetized mice were intranasally immunized with 5 μg of SARS-CoV-2 S protein trimer and 0.1 μg of cholera toxin in 10 μl of PBS by using a pipette to deliver the fluid dropwise into each nostril a total of 3 times at 3-week intervals. One week after the final immunization, *mi*ce were sacrificed by CO_2 inhalation, and blood samples were collected from the inferior vena cava. To avoid contamination with circulating blood lymphocytes, the mice were perfused with 2 ml of PBS via the heart. Then, the lungs, the spleen, bone marrow and Peyer's patches were dissected, and single-cell suspensions were obtained by mincing the tissue using a 100-μm nylon mesh. The mice were decapitated at the larynx. After the removal of the facial skin from the head, the nose was separated from the rest of the head. A pipette tip was inserted through the pharyngeal opening into the choana, and then two consecutive volumes of 250 μl of PBS were gently perfused, and the nostril fluid was collected in a tube. The nasal lavage fluids were centrifuged, and

supernatants were stored at −80°C until assayed. The isolated nose was cut into two along the midline, the layer of epithelium was mechanically removed from the nasal septum by gently rubbing the sample with a needle under a stereoscopic microscope, and the tissues were then mechanically shredded. Single-cell suspensions containing lymphocytes were isolated by using Lympholyte-M (Cedar Lane, Ontario, Canada).

ELISA

ELISA to evaluate antibody binding to the S-trimer, RBDs or NTD was performed by coating Nunc MaxiSorp flat-bottom high-binding 96-half-well plates (ThermoFisher Scientific, MS, USA) with 50 μl per well of a 0.1 μg ml^{-1} protein solution in PBS overnight at 4 °C. Plates were washed 3 times with PBS and incubated with 170 μl per well Blocking One solution (Nakarai, Tokyo, Japan) for 1 h at room temperature. Serially diluted antibody, serum or nasal lavage field was added to PBST (1× PBS with 0.1% Tween-20) and incubated for 1 h at room temperature. The plates were washed three times with PBST and then incubated with anti-mouse IgG or IgA secondary antibody conjugated to horseradish peroxidase (HRP) (Abcam, Cambridge, UK) in PBST for 1 h at room temperature. After washing with PBST 3 times, the plates were developed by addition of the SureBlue/TMB peroxidase substrate and stop solution (KPL, MS, USA), and absorbance was measured at 450 nm with an ELISA microplate reader. Serum and nasal fluid antibody titers were also determined ELISA. 96-well plates coated with 1 μg of anti-mouse IgA or IgG were blocked with Blocking One solution. Samples were diluted with PBST and incubated for 1 h at room temperature. After washing, 100 μL alkaline phosphatase-conjugated anti-mouse IgA or anti-mouse IgG was added to each well and incubated for 1 h at room temperature. Plates were washed and developed with BluePhos Microwell Substrate Kit (KPL, MS, USA). Mouse IgA or IgG was used as a reference to construct a standard curve for quantifying antibodies.

ACE2 blocking assay.

Nunc Maxisorp plates were coated with SARS-CoV-2 RBD at 50 ng per well and incubated overnight at 4°C. After blocking with Blocking One solution for 1 h at room temperature, serially diluted antibody mixed with 5 ng of biotinylated ACE2 in 100 μL of PBST was transferred to the plate in triplicate. After incubation for 1 h at room temperature, the assay plate was washed with PBST three times, and 100 μL of streptavidin-HRP (Abcam, Cambridge, UK) diluted 1:5000 in PBST was transferred to each well and incubated for 30 min. After three washes, the plate was developed with streptavidin-HRP and SureBlue/TMB peroxidase substrate.

Plasmid construction

The DNA fragments encoding the human IgA2 constant region, human J-chain and extracellular domain of

human pIgR were amplified by PCR. The IgA2 constant region was replaced with the IgG1 constant region of pJON-mIgG or pETmIgA to make pJON-hIgA and pET-hIgA, respectively (*Kurosawa et al. , 2012*). The human J chain was replaced with the DsRed2 gene of pDsRedN1 (Takara Bio, Shiga, Japan). The pIgR gene was inserted into the pEF-Myc-His vector (ThermoFisher Scientific, MS, USA).

Isolation of antigen-specific plasma cells

Isolation of antigen-specific plasma cells was performed as described previously with slight modifications (*Kurosawa et al. , 2012*). Nasal lymphoid cells or splenocytes were stained with PE-labeled anti-mouse CD138, DyLight-650-labeled S1 and DyLight488-labeled anti-mouse IgA or anti-mouse IgG at 4°C for 30 min with gentle agitation. After washing with PBS, the cells were suspended in PBS containing ER-tracker and subsequently analyzed by FACS. The forward-versus-side-scatter (FSC vs. SSC) lymphocyte gate (R1) was applied to exclude dead cells. The plasma cells (IgGA+, CD138+, ERhigh, R2 gate) were further subdivided into fractions according to their binding of fluorescently labeled SARS-CoV-2 to define antigen-specific plasma cells (IgA+, ERhigh SARS+). Single-cell sorting was performed using a JSAN Cell Sorter that was equipped with an automatic cell deposition unit (JSAN, Kobe, Japan) with DyLight488-labeled antibodies against IgA monitored in the FL-l channel, PE-labeled CD138 in the FL-2 channel, ER-tracker in the FL-7 channel and DyLight650-labeled SARS-COV-2 in the FL-6 channel.

Monoclonal antibody generation

Molecular cloning of VH and VL genes from single cells was performed by 5'-RACE PCR as previously described. For the first antibody screening, the PCR-amplified VHa and VL genes were joined to pJON-hIgA and pJON-mIgK to make full-length immunoglobulin alpha heavy and kappa light chain genes by TS-jPCR, respectively (*Yoshioka et al. , 2011*). M-IgA was expressed by transfecting a pair of alpha heavy and kappa light chain genes into FreeStyle CHO-S cells that were grown in a 24-well plate according to the manufacturer's protocol (CHOgro High Yield Expression System, Takara Bio, Shiga, Japan). For large-scale antibody production, the PCR-amplified alpha heavy and kappa light chain genes were inserted into pET-hIgA and pET-mIgK by TS-HR, respectively (*Kurosawa et al. , 2011*).

M-IgA was expressed by cotransfecting plasmids encoding the IgA gene (5 μg) and IgK gene (5 μg) into FreeStyle™ CHO-S cells (2.0×10^5 cells/10 ml). S-IgA was expressed by cotransfecting plasmids encoding the IgA gene (5 μg), IgK gene (5 μg), J-chain (1 μg) and pIgR gene (1 μg) into FreeStyle™ CHO-S cells (2.0×10^5 cells/10 ml). M-IgA was purified by using Peptide M Agarose (ThermoFisher Scientific). S-IgA was purified by two-step chromatography using the Capturem His-Taged Purification Kit (Takara Bio, Shiga, Japan) followed by size exclusion chromatography (Cytiva, Acta go, MS, USA). The purified antibodies were analyzed by SDS–PAGE and native polyacrylamide gel electrophoresis on NuPAGE 4–

12% Bis-Tris gels (Thermo Fisher Scientific MS, USA).

Antibody binding kinetics by SPR

The binding kinetics and affinity of monoclonal antibodies to the SARS-CoV-2 spike trimer were analyzed by SPR (Biacore T100, GE Healthcare). Specifically, a biotinylated spike trimer was covalently immobilized to an SA Sensor Chip for a final RU of approximately 200 and interacted with M-IgA or S-IgA at various concentrations (0.3, 1.0, 3.0, 9.0 and 27 nM of each antibody). SPR assays were run at a flow rate of 30 µl/min in HEPES buffer. The dissociation phase was monitored for 5 minutes. The sensograms were fit in a two-component model with BIA Evaluation software (GE Healthcare).

Neutralization activity of monoclonal antibodies against pseudotyped SARS-CoV-2 virus

VeroE6/TMPRSS2 cells were incubated with serially diluted antibodies and pseudotyped virus possessing the spike protein of the Wuhan, Delta, Omicron strains or vesicular stomatitis virus (VSV) and cultured for 48 h at 37°C. After exposure to the virus–antibody mixture, the infectivity of the pseudotyped viruses was determined by measuring the luciferase activities using a PicaGene Luminescence Kit (Fujifilm Wako, Osaka, Japan) with a GloMax Navigator Microplate Luminometer (Promega, WI, USA).

Neutralization assay using an authentic virus strain.

The neutralizing activity of monoclonal antibodies against an authentic Wuhan SARS-CoV-2 strain was determined by a neutralization test in a biosafety level 3 laboratory at the Toyama Institute of Health as previously described (*Ozawa et al. , 2022*). VeroE6/TMPRSS2 cells plated at 2×10^4 cells in each well of 96-well plates were infected with the Wuhan SARS-CoV-2 strain at a multiplicity of infection of 0.001 per cell in the presence of serially 2-fold diluted monoclonal antibodies for 1 h. After discarding the culture supernatants, cells were cultured for 24 h with DMEM containing 10% FBS in the presence of the indicated concentration of monoclonal antibodies. The viral infectious dose was determined by the level of viral genomic RNA in the culture supernatant, which was measured using a real-time PCR assay with a SARS-CoV-2 direct detection RT–qPCR kit (Takara Bio, Siga, Japan). The IC_{50} was calculated by IC50 Calculator (https://www.aatbio.com/tools/ic50-calculator) and represented the neutralization titer.

Gene family and phylogenetic analysis of monoclonal antibodies

The antibody sequences were annotated against the IMGT mouse heavy and light chain gene database using NCBI IgBlast to determine IGHV, IGHD, IGLV, IGHJ, IGLV and IGLJ gene annotations. Antibody clones were assigned to clonal groups using Sequencher software. The heavy and light chain variable gene arrangement and phylogenetic analyses were performed using MAFFT, a multiple alignment program, in

the GENETYX sequence analysis package (https://www.genetyx.co.jp). For somatic hypermutation, IGHV and IGLV sequences were aligned against representative clones of each group. Antibody clones consisting of pairs of heavy and light chain variable genes (signal sequence to FW4) were used to generate an antibody phylogenetic tree. Full-length germline sequences were reconstructed, with nucleotide additions/deletions in the junction between V-(D)-J adjusted to match the sequence of each antibody group. Within these groups, if the combined sequence of the heavy and light chains differed by more than five bases from each other, they were defined as separate clones. The sequence alignment tool Clustal Omega (https://www.ebi.ac.uk/Tools/msa/clustalo/) was used to identify deletions and insertions and to align the length of the sequence. The nucleotide lengths were aligned by adding "-" to the missing bases. The data file required by Alakazam was created in RStudio (version 2022.12.0+353), and a phylogenetic tree was created by Alakazam (https://www.rdocumentation.org/packages/alakazam/versions/1.2.1 and https://alakazam.readthedocs.io/en/stable/). The R script was as follows: https://www.rdocumentation.org/packages/alakazam/versions/1.2.1/topics/buil dPhylipLineage

Statistical analysis

All statistical analyses were performed using JMP statistical software (JMP Statistical Discovery, NC, USA). Unpaired Student's t tests were used to analyze each dataset. The threshold for statistical significance was set at $p < 0.01$ (**).

Data availability

The nucleotide sequence data were submitted to the DDBJ/EMBL/GenBank databases (Accession No. LC761389 ~ LC761570). Other relevant data are available from the corresponding authors upon request.

Acknowledgments

We thank past and current members of our laboratory for fruitful discussions. We also thank M. Nozaki and K. Takai for technical support.

References

Afkhami S, D'Agostino MR, Zhang A, Stacey HD, Marzok A, Kang A, Singh R, Bavananthasivam J, Ye G, Luo X, Wang F, Ang JC, Zganiacz A, Sankar U, Kazhdan N, Koenig JFE, Phelps A, Gameiro SF, Tang S, Jordana M, Wan Y, Mossman KL, Jeyanathan M, Gillgrass A, Medina MFC, Smaill F, Lichty BD, Miller MS, Xing Z. 2022. Respiratory mucosal delivery of next-generation COVID-19 vaccine provides robust protection against both ancestral and variant strains of SARS-CoV-2. *Cell* **185**:896-915 e819. DOI: 10.1016/j.cell.2022.02.005, PMID: PMC8825346

Alu A, Chen L, Lei H, Wei Y, Tian X, Wei X. 2022. Intranasal COVID-19 vaccines: From bench to bed. *EBioMedicine* **76**:103841. DOI: 10.1016/j.ebiom.2022.103841, PMID: PMC8785603

Asahi Y, Yoshikawa T, Watanabe I, Iwasaki T, Hasegawa H, Sato Y, Shimada S, Nanno M, Matsuoka Y, Ohwaki M, Iwakura Y, Suzuki Y, Aizawa C, Sata T, Kurata T, Tamura S. 2002. Protection against influenza virus infection in polymeric Ig receptor knockout mice immunized intranasally with adjuvant-combined vaccines. *J Immunol* **168**:2930-2938. DOI: 10.4049/jimmunol.168.6.2930

Asahi-Ozaki Y, Yoshikawa T, Iwakura Y, Suzuki Y, Tamura S, Kurata T, Sata T. 2004. Secretory IgA antibodies provide cross-protection against infection with different strains of influenza B virus. *J Med Virol* **74**:328-335. DOI: 10.1002/jmv.20173

Azzi L, Dalla Gasperina D, Veronesi G, Shallak M, Ietto G, Iovino D, Baj A, Gianfagna F, Maurino V, Focosi D, Maggi F, Ferrario MM, Dentali F, Carcano G, Tagliabue A, Maffioli LS, Accolla RS, Forlani G. 2022. Mucosal immune response in BNT162b2 COVID-19 vaccine recipients. *EBioMedicine* **75**:103788. DOI: 10.1016/j.ebiom.2021.103788, PMID: PMC8718969

Barrett JR, Belij-Rammerstorfer S, Dold C, Ewer KJ, Folegatti PM, Gilbride C, Halkerston R, Hill J, Jenkin D, Stockdale L, Verheul MK, Aley PK, Angus B, Bellamy D, Berrie E, Bibi S, Bittaye M, Carroll MW, Cavell B, Clutterbuck EA, Edwards N, Flaxman A, Fuskova M, Gorringe A, Hallis B, Kerridge S, Lawrie AM, Linder A, Liu X, Madhavan M, Makinson R, Mellors J, Minassian A, Moore M, Mujadidi Y, Plested E, Poulton I, Ramasamy MN, Robinson H, Rollier CS, Song R, Snape MD, Tarrant R, Taylor S, Thomas KM, Voysey M, Watson MEE, Wright D, Douglas AD, Green CM, Hill AVS, Lambe T, Gilbert S, Pollard AJ, Oxford CVTG. 2021. Phase 1/2 trial of SARS-CoV-2 vaccine ChAdOx1 nCoV-19 with a booster dose induces multifunctional antibody responses. *Nat Med* **27**:279-288. DOI: 10.1038/s41591-020-01179-4

Bricker TL, Darling TL, Hassan AO, Harastani HH, Soung A, Jiang XP, Dai YN, Zhao HY, Adams LJ, Holtzman MJ, Bailey AL, Case JB, Fremont DH, Klein R, Diamond MS, Boon ACM. 2021. A single intranasal or intramuscular immunization with chimpanzee adenovirus-vectored SARS-CoV-2 vaccine protects against pneumonia in hamsters. *Cell Reports* **36**. DOI: ARTN 109400 10.1016/j.celrep.2021.109400

Budinger GRS, Misharin AV, Ridge KM, Singer BD, Wunderink RG. 2021. Distinctive features of severe SARS-CoV-2 pneumonia. *J Clin Invest* **131**. DOI: 10.1172/JCI149412, PMID: PMC8279580

Callegari I, Schneider M, Berloffa G, Muhlethaler T, Holdermann S, Galli E, Roloff T, Boss R, Infanti L, Khanna N, Egli A, Buser A, Zimmer G, Derfuss T, Sanderson NSR. 2022. Potent neutralization by monoclonal human IgM against SARS-CoV-2 is impaired by class switch. *EMBO Rep* **23**:e53956. DOI: 10.15252/embr.202153956, PMID: PMC9253785

Chavda VP, Vora LK, Pandya AK, Patravale VB. 2021. Intranasal vaccines for SARS-CoV-2: From challenges to potential in COVID-19 management. *Drug Discov Today* **26**:2619-2636. DOI: 10.1016/j.drudis.2021.07.021, PMID: PMC8319039

D'Arco C, McCormick AA, Arnaboldi PM. 2021. Single-dose intranasal subunit vaccine rapidly clears secondary sepsis in a high-dose pneumonic plague infection. *Vaccine* **39**:1435-1444. DOI: 10.1016/j.vaccine.2021.01.040

DeFrancesco L. 2020. COVID-19 antibodies on trial. *Nat Biotechnol* **38**:1242-1252. DOI: 10.1038/s41587-020-0732-8, PMID: PMC7576980

Dhakal S, Renu S, Ghimire S, Shaan Lakshmanappa Y, Hogshead BT, Feliciano-Ruiz N, Lu F, HogenEsch H, Krakowka S, Lee CW, Renukaradhya GJ. 2018. Mucosal Immunity and Protective Efficacy of Intranasal Inactivated Influenza Vaccine Is Improved by Chitosan Nanoparticle Delivery in Pigs. *Front Immunol* **9**:934. DOI: 10.3389/fimmu.2018.00934, PMID: PMC5940749

Ejemel M, Li Q, Hou S, Schiller ZA, Tree JA, Wallace A, Amcheslavsky A, Kurt Yilmaz N, Buttigieg KR, Elmore MJ, Godwin K, Coombes N, Toomey JR, Schneider R, Ramchetty AS, Close BJ, Chen DY, Conway HL, Saeed M, Ganesa C, Carroll MW, Cavacini LA, Klempner MS, Schiffer CA, Wang Y. 2020. A cross-reactive human IgA monoclonal antibody blocks SARS-CoV-2 spike-ACE2 interaction. *Nat Commun* **11**:4198. DOI: 10.1038/s41467-020-18058-8, PMID: PMC7442812

Galimidi RP, Klein JS, Politzer MS, Bai S, Seaman MS, Nussenzweig MC, West AP, Jr., Bjorkman PJ. 2015. Intra-spike crosslinking overcomes antibody evasion by HIV-1. *Cell* **160**:433-446. DOI: 10.1016/j.cell.2015.01.016, PMID: PMC4401576

Gianchecchi E, Manenti A, Kistner O, Trombetta C, Manini I, Montomoli E. 2019. How to assess the effectiveness of nasal influenza vaccines? Role and measurement of sIgA in mucosal secretions. *Influenza and Other Respiratory Viruses* **13**:429-437. DOI: 10.1111/irv.12664

Houston S. 2023. SARS-CoV-2 mucosal vaccine. *Nat Immunol* **24**:1. DOI: 10.1038/s41590-022-01405-w

Jackson CB, Farzan M, Chen B, Choe H. 2022. Mechanisms of SARS-CoV-2 entry into cells. *Nat Rev Mol Cell Biol* **23**:3-20. DOI: 10.1038/s41580-021-00418-x, PMID: PMC8491763

Kim E, Weisel FJ, Balmert SC, Khan MS, Huang SH, Erdos G, Kenniston TW, Carey CD, Joachim SM, Conter LJ, Weisel NM, Okba NMA, Haagmans BL, Percivalle E, Cassaniti I, Baldanti F, Korkmaz E, Shlomchik MJ, Falo LD, Gambotto A. 2021. A single subcutaneous or intranasal immunization with adenovirus-based SARS-CoV-2 vaccine induces robust humoral and cellular immune responses in mice. *European Journal of Immunology* **51**:1774-1784. DOI: 10.1002/eji.202149167

Klein JS, Bjorkman PJ. 2010. Few and far between: how HIV may be evading antibody avidity. *PLoS Pathog* **6**:e1000908. DOI: 10.1371/journal.ppat.1000908, PMID: PMC2877745

Kurosawa N, Yoshioka M, Fujimoto R, Yamagishi F, Isobe M. 2012. Rapid production of antigen-specific monoclonal antibodies from a variety of animals. *Bmc Biology* **10**. DOI: Artn 80,10.1186/1741-7007-10-80

Kurosawa N, Yoshioka M, Isobe M. 2011. Target-selective homologous recombination cloning for high-throughput generation of monoclonal antibodies from single plasma cells. *Bmc Biotechnology* **11**. DOI: Artn 39,10.1186/1472-6750-11-39

Lapuente D, Fuchs J, Willar J, Vieira Antao A, Eberlein V, Uhlig N, Issmail L, Schmidt A, Oltmanns F, Peter AS, Mueller-Schmucker S, Irrgang P, Fraedrich K, Cara A, Hoffmann M, Pohlmann S, Ensser A, Pertl C, Willert T, Thirion C, Grunwald T, Uberla K, Tenbusch M. 2021. Protective mucosal immunity against SARS-CoV-2 after heterologous systemic prime-mucosal boost immunization. *Nat Commun* **12**:6871. DOI: 10.1038/s41467-021-27063-4, PMID: PMC8626513

Li Y, Jin L, Chen T. 2020. The Effects of Secretory IgA in the Mucosal Immune System. *Biomed Res Int* **2020**:2032057. DOI: 10.1155/2020/2032057, PMID: PMC6970489

Maltseva M, Galipeau Y, Renner TM, Deschatelets L, Durocher Y, Akache B, Langlois MA. 2022. Characterization of Systemic and Mucosal Humoral Immune Responses to an Adjuvanted Intranasal SARS-CoV-2 Protein Subunit Vaccine Candidate in Mice. *Vaccines (Basel)* **11**. DOI: 10.3390/vaccines11010030, PMID: PMC9865305

Matsumoto ML. 2022. Molecular Mechanisms of Multimeric Assembly of IgM and IgA. *Annu Rev Immunol*. DOI: 10.1146/annurev-immunol-101320-123742

Nicasio M, Sautto G, Clementi N, Diotti RA, Criscuolo E, Castelli M, Solforosi L, Clementi M, Burioni R. 2012. Neutralization interfering antibodies: a "novel" example of humoral immune dysfunction facilitating viral escape? *Viruses* **4**:1731-1752. DOI: 10.3390/v4091731, PMID: PMC3499828

Ohtsuka J, Imai M, Fukumura M, Maeda M, Eguchi A, Ono R, Maemura T, Ito M, Yamayoshi S, Kataoka Y, Kawaoka Y, Nosaka T. 2021. Non-propagative human parainfluenza virus type 2 nasal vaccine robustly protects the upper and lower airways against SARS-CoV-2. *iScience* **24**:103379. DOI: 10.1016/j.isci.2021.103379, PMID: PMC8596570

Okuya K, Eguchi N, Manzoor R, Yoshida R, Saito S, Suzuki T, Sasaki M, Saito T, Kida Y, Mori-Kajihara A, Miyamoto H, Ichii O, Kajihara M, Higashi H, Takada A. 2020a. Comparative Analyses of the Antiviral Activities of IgG and IgA Antibodies to Influenza A Virus M2 Protein. *Viruses* **12**. DOI: 10.3390/v12070780, PMID: PMC7411592

Okuya K, Yoshida R, Manzoor R, Saito S, Suzuki T, Sasaki M, Saito T, Kida Y, Mori-Kajihara A, Kondoh T, Sato M, Kajihara M, Miyamoto H, Ichii O, Higashi H, Takada A. 2020b. Potential Role of Nonneutralizing IgA Antibodies in Cross-Protective Immunity against Influenza A Viruses of Multiple Hemagglutinin Subtypes. *Journal of Virology* **94**. DOI: ARTN e00408-20 10.1128/JVI.00408-20

Ozawa T, Tani H, Anraku Y, Kita S, Igarashi E, Saga Y, Inasaki N, Kawasuji H, Yamada H, Sasaki SI, Somekawa M, Sasaki J, Hayakawa Y, Yamamoto Y, Morinaga Y, Kurosawa N, Isobe M, Fukuhara H, Maenaka K, Hashiguchi T, Kishi H, Kitajima I, Saito S, Niimi H. 2022. Novel super-neutralizing antibody UT28K is capable of protecting against infection from a wide variety of SARS-CoV-2 variants. *MAbs* **14**:2072455. DOI: 10.1080/19420862.2022.2072455, PMID: PMC9103358

Polack FP, Thomas SJ, Kitchin N, Absalon J, Gurtman A, Lockhart S, Perez JL, Perez Marc G, Moreira ED, Zerbini C, Bailey R, Swanson KA, Roychoudhury S, Koury K, Li P, Kalina WV, Cooper D, Frenck RW, Jr., Hammitt LL, Tureci O, Nell H, Schaefer A, Unal S, Tresnan DB, Mather S, Dormitzer PR, Sahin U, Jansen KU, Gruber WC, Group CCT. 2020. Safety and Efficacy of the BNT162b2 mRNA Covid-19 Vaccine. *N Engl J Med* **383**:2603-2615. DOI: 10.1056/NEJMoa2034577, PMID: PMC7745181

Saito S, Sano K, Suzuki T, Ainai A, Taga Y, Ueno T, Tabata K, Saito K, Wada Y, Ohara Y, Takeyama H, Odagiri T, Kageyama T, Ogawa-Goto K, Multihartina P, Setiawaty V, Pangesti KNA, Hasegawa H. 2019. IgA tetramerization improves target breadth but not peak potency of functionality of anti-influenza virus broadly neutralizing antibody. *PLoS Pathog* **15**:e1007427. DOI: 10.1371/journal.ppat.1007427, PMID: PMC6317788

Sheikh-Mohamed S, Isho B, Chao GYC, Zuo M, Cohen C, Lustig Y, Nahass GR, Salomon-Shulman RE, Blacker G, Fazel-Zarandi M, Rathod B, Colwill K, Jamal A, Li Z, de Launay KQ, Takaoka A, Garnham-Takaoka J, Patel A, Fahim C, Paterson A, Li AX, Haq N, Barati S, Gilbert L, Green K, Mozafarihashjin M, Samaan P, Budylowski P, Siqueira WL, Mubareka S, Ostrowski M, Rini JM, Rojas OL, Weissman IL, Tal MC, McGeer A, Regev-Yochay G, Straus S, Gingras AC, Gommerman JL. 2022. Systemic and mucosal IgA responses are variably induced in response to SARS-CoV-2 mRNA vaccination and are associated with protection against subsequent infection. *Mucosal Immunol* **15**:799-808. DOI: 10.1038/s41385-022-00511-0, PMID: PMC9037584

Shimoda M, Nakamura T, Takahashi Y, Asanuma H, Tamura S, Kurata T, Mizuochi T, Azuma N, Kanno C, Takemori T. 2001. Isotype-specific selection of high affinity memory B cells in nasal-associated lymphoid tissue. *Journal of Experimental Medicine* **194**:1597-1607. DOI: DOI 10.1084/jem.194.11.1597

Sterlin D, Malaussena A, Gorochov G. 2021. IgA dominates the early neutralizing antibody response to SARS-CoV-2 virus. *M S-Medecine Sciences* **37**:968-970. DOI: 10.1051/medsci/2021154

Sui Y, Li J, Zhang R, Prabhu SK, Andersen H, Venzon D, Cook A, Brown R, Teow E, Velasco J, Greenhouse J, Putman-Taylor T, Campbell TA, Pessaint L, Moore IN, Lagenaur L, Talton J, Breed MW, Kramer J, Bock KW, Minai M, Nagata BM, Lewis MG, Wang LX, Berzofsky JA. 2021. Protection against SARS-CoV-2 infection by a mucosal vaccine in rhesus macaques. *JCI Insight* **6**. DOI: 10.1172/jci.insight.148494, PMID: PMC8262352

Sungnak W, Huang N, Becavin C, Berg M, Queen R, Litvinukova M, Talavera-Lopez C, Maatz H, Reichart D, Sampaziotis F, Worlock KB, Yoshida M, Barnes JL, Network HCALB. 2020. SARS-CoV-2 entry factors are highly expressed in nasal epithelial cells together with innate immune genes. *Nat Med* **26**:681-687. DOI: 10.1038/s41591-020-0868-6, PMID: PMC8637938

Tan GS, Leon PE, Albrecht RA, Margine I, Hirsh A, Bahl J, Krammer F. 2016. Broadly-Reactive Neutralizing and Non-neutralizing Antibodies Directed against the H7 Influenza Virus Hemagglutinin Reveal Divergent Mechanisms of Protection. *PLoS Pathog* **12**:e1005578. DOI: 10.1371/journal.ppat.1005578, PMID: PMC4833315

Tumpey TM, Renshaw M, Clements JD, Katz JM. 2001. Mucosal delivery of inactivated influenza vaccine induces B-cell-dependent heterosubtypic cross-protection against lethal influenza A H5N1 virus infection. *J Virol* **75**:5141-5150. DOI: 10.1128/JVI.75.11.5141-5150.2001, PMID: PMC114919

Vabret N, Britton GJ, Gruber C, Hegde S, Kim J, Kuksin M, Levantovsky R, Malle L, Moreira A, Park MD, Pia L, Risson E, Saffern M, Salome B, Esai Selvan M, Spindler MP, Tan J, van der Heide V, Gregory JK, Alexandropoulos K, Bhardwaj N, Brown BD, Greenbaum B, Gumus ZH, Homann D, Horowitz A, Kamphorst AO, Curotto de Lafaille MA, Mehandru S, Merad M, Samstein RM, Sinai Immunology Review P. 2020. Immunology of COVID-19: Current State of the Science. *Immunity* **52**:910-941. DOI: 10.1016/j.immuni.2020.05.002, PMID: PMC7200337

Wong TY, Lee KS, Russ BP, Horspool AM, Kang J, Winters MT, Allison Wolf M, Rader NA, Miller OA, Shiflett M, Izac J, Varisco D, Sen-Kilic E, Cunningham C, Cooper M, Cyphert HA, Barbier M, Martinez I, Bevere JR, Ernst RK, Damron FH. 2022. Intranasal administration of BReC-CoV-2 COVID-19 vaccine protects K18-hACE2 mice against lethal SARS-CoV-2 challenge. *NPJ Vaccines* **7**:36. DOI: 10.1038/s41541-022-00451-7

Woof JM, Kerr MA. 2006. The function of immunoglobulin A in immunity. *J Pathol* **208**:270-282. DOI: 10.1002/path.1877

1 Yoshioka M, Kurosawa N, Isobe M. 2011. Target-selective joint polymerase chain reaction: A robust and
2 rapid method for high-throughput production of recombinant monoclonal antibodies from single
3 cells. *Bmc Biotechnology* **11**. DOI: 10.1186/1472-6750-11-75